CHEMISTRY OF MATERIALS
Article

Chem. Mater. **2009,** *21,* 5627–5636 5627
DOI:10.1021/cm9021326

Nanoseashells and Nanooctahedra of MoS_2: Routes to Inorganic Fullerenes

Andrey N. Enyashin,*[,†,‡,⊥] Maya Bar-Sadan,*[,§,⊥] Jeremy Sloan,[∥] Lothar Houben,[§] and Gotthard Seifert[†]

[†]*Physikalische Chemie, Technische Universität Dresden, D-01062 Dresden, Germany,* [‡]*Institute of Solid State Chemistry UB RAS, GSP-145, 620990 Ekaterinburg, Russia,* [§]*Institute of Solid State Research and Ernst Ruska Centre for Microscopy and Spectroscopy with Electrons, Forschungszentrum Jülich GmbH, 52425 Jülich, Germany, and* [∥]*Department of Physics, University of Warwick, Coventry, Warwickshire CV4 7AL, U.K.* [⊥] *These authors contributed equally to this work.*

Received July 14, 2009. Revised Manuscript Received September 28, 2009

Nanooctahedra of MoS_2 are considered to be the true inorganic fullerenes, exhibiting different properties from the bulk and also other closed-cage morphologies of the same material. These structures are produced in high energy systems where the synthesis is performed far from equilibrium conditions, and the reaction mechanism involved remains unknown. Here, the discovery of two imperfect structures of nanooctahedra—the distorted octahedra and seashell structures with meander-like cross sections—is reported and studied in detail using transmission electron microscopy and quantum-mechanical methods. These nanoparticles can serve to understand the synthesis route by establishing the basic principles of their morphology and stability. The fundamental properties of the inorganic lattice are the basis for matching the projections observed in microscopy images with a suggested atomistic model. Quantum-mechanical calculations are used to estimate their stability and electronic properties. It was concluded that the production of nanooctahedra involves a high temperature stage, where lattice defects enable the formation of a closed structure without a templating particle. Thereafter at lower temperatures, the mixture of products is carried forward and the annealing contributes to the enrichment of the product with more symmetric structures.

1. Introduction

Inorganic closed cage structures that are analogous in structure to those of the carbon fullerene family are being synthesized in ever larger quantities and from an increasing variety of compounds.[1,2] Among these, nanoparticles and nanotubes prepared from WS_2 and MoS_2 are among the most remarkable in terms of their physical characteristics, in particular regarding their lubrication, antiwear properties, and comparative ease of synthesis. Consequently, they are now prepared in semitonnage quantities and are being exploited for commercial applications. WS_2 and MoS_2 were also the first noncarbon compounds that were observed as fullerene-like nanoparticles with onion-like architecture (designated IF) and as multiwall nanotube-type structures (denoted INT).[3] The spheroidal or tube-like morphology results in a lower density of dangling bonds in comparison to non-IF particulates of the bulk material, allowing for a significant increase in terms of the antifrictional characteristics. As a result, IF WS_2 and MoS_2 particles are now one of the basic components for technical lubricants with higher resistance in either a humid or an oxidative environment. Therefore, both tribological properties and the structural evolution of such particles are a major focus of experimental and theoretical research.[4−9]

The analogy of inorganic nanostructures based on layered materials to carbon nanostructures is only approximate, since inorganic fullerene-like and nanotubular structures do not contain just a single element but are compounds which contain two or more elements. As a result, the structural mechanism which enables the folding and closing of a single shell structure into a closed cage structure is fundamentally different. The closest analogy to carbon is BN, which forms the same graphene-like structure but with alternating atoms of boron and nitrogen. Like carbon, BN forms layered phases, where each

*Corresponding author. E-mail: enyashin@ihim.uran.ru.

(1) Tenne, R. *Nat. Nanotechnol.* **2006**, *1*, 103–111.
(2) Enyashin, A. N.; Gemming, S.; Bar-Sadan, M.; Popovitz-Biro, R.; Hong, S. Y.; Prior, Y.; Tenne, R.; Seifert, G. *Angew. Chem., Int. Ed.* **2007**, *46*, 623–627.
(3) Tenne, R.; Margulis, L.; Genut, M.; Hodes, G. *Nature* **1992**, *360*, 444–446.
(4) Rapoport, L.; Bilik, Y.; Feldman, Y.; Homyonfer, M.; Cohen, S. R.; Tenne, R. *Nature* **1997**, *387*, 791–793.
(5) Rapoport, L.; Leshchinsky, V.; Lapsker, I.; Volovik, Y.; Nepomnyashchy, O.; Lvovsky, M.; Popovitz-Biro, R.; Feldman, Y.; Tenne, R. *Wear* **2003**, *255*, 785–793.
(6) Rapoport, L.; Lvovsky, M.; Lapsker, I.; Leshchinsky, V.; Volovik, Y.; Feldman, Y.; Margolin, A.; Rosentsveig, R.; Tenne, R. *Nano Lett.* **2001**, *1*, 137–140.
(7) Rapoport, L.; Nepomnyashchy, O.; Lapsker, I.; Verdyan, A.; Soifer, Y.; Popovitz-Biro, R.; Tenne, R. *Tribology Lett.* **2005**, *19*, 143–149.
(8) Hu, J. J.; Zabinski, J. S. *Tribology Lett.* **2005**, *18*, 173–180.
(9) Stefanov, M.; Enyashin, A. N.; Heine, T.; Seifert, G. *J. Phys. Chem. C* **2008**, *112*, 17764–17767.

Published on Web 10/27/2009

layer consists of hexagons, and also a diamond-like phase, which is less stable at room temperature. In contrast to carbon, however, BN easily forms highly faceted nested structures.[10,11] Calculations show that B−B or N−N bonds are energetically unfavorable, preventing the formation of odd-numbered rings in the hexagonal bulk structure.[12] The result is a rectangular ring of B and N dictating the faceted 3D hollow structure and, in its basic shape, an octahedron (i.e., a rectangular bipyramid).

Discrete cage structures also exist in the smallest sized nanoparticles formed from layered sulfides: MoS_2, $MoSe_2$, and WS_2. These so-called "true" inorganic fullerenes (as opposed to onion-like nanoparticles) are composed of a few layers in the shape of concentric octahedra with an edge size of the order of 5 nm.[13] MoS_2 and $MoSe_2$ form nanooctahedra when produced by high-energy synthetic methods such as laser ablation,[2,13−15] and the three-dimensional structure of these nanooctahedra was rigorously verified by electron tomography in ultrahigh resolution transmission electron microscopy (HRTEM).[16] Recently, ab initio computational methods have been adopted to describe their construction principles on an atomic basis and also to make predictions about their comparative stability.[2,15] The unique octahedron morphology of inorganic fullerenes has been explained by the appearance of six ordered square-like defects within the hexagonal lattice of a dichalcogenide monolayer leading to the formation of the fullerene corners. Preliminary quantum-mechanical calculations have also shown that small octahedral fullerenes of MoS_2 have a metallic-like character in their electronic density of states despite the semiconducting nature of the bulk and the nanotubular material.[2,15] The calculations suggest that octahedral MoS_2 and the related WS_2 nanoparticles may demonstrate catalytic properties, similar to the respective nanosized bulk material or monolayered nanoplatelets deposited on a metal surface. Taking into account the fact that octahedral sulfide fullerenes become more stable than nanoplatelets below a particle size of a few nanometers ($< 12\,000$ atoms),[15] there is also a motivation to exploit them in the future as candidate nanomaterials for catalytic fuel desulfurization. At present, "true" inorganic fullerenes can be found only in the soot of the respective compound collected following the processes of laser ablation, solar-beam ablation,[17] or arc-discharge[18] when the respective bulk is used as the pristine material. Theoretical studies predict that other compounds (e.g., TiO_2) could also appear as nanooctahedra;[19] therefore, most likely this structural characteristic is not a unique property of dichalcogenides.

To improve the yield of inorganic fullerenes, it is essential to learn more about the reaction mechanism and also the kinetics of the formation process. High-energy-density/high-power processes such as laser ablation and arc discharge are characterized far from equilibrium conditions such as high temperatures and short reaction times. The nonequilibrium conditions of formation and the instability of the intermediate products, which prevents their isolation, have made it difficult to arrive at a single explanation of the reaction path. This is the case even in the carbon fullerene family where the structures are as small as 60 identical atoms.

Other publications[18,20] and our own experience also show experimental TEM images which are neither rhombic nor hexagonal projections and therefore cannot be attributed to the symmetric octahedral structure. To improve the control of the synthesis, it is important to correlate the imperfect structures which are found in the soot with a suggested reaction mechanism that would explain the symmetric structures as well as the distorted ones. In the present work, we take a detailed look at the morphology of nanoparticles obtained in the soots of MoS_2 and $MoSe_2$ after laser ablation using electron microscopy methods. We report the discovery of two imperfect structures of nanooctahedra: the distorted octahedra and the seashell-like structures. Atomistic models of the respective MoS_2 nanoparticles and quantum-mechanical calculations are used to establish basic principles concerning the stability and electronic properties of distorted nanooctahedra and nanoseashells of MoS_2. From this evidence, a reaction mechanism is suggested and discussed.

2. Experimental Section

Synthesis. MoS_2 powder (Sigma Aldrich, 99.5% pure) was pressed into a target pellet (diameter 17 mm). The target was placed inside a quartz tube reactor heated to 720−970 K. Pulsed laser ablation was conducted using a mildly focused, frequency-doubled Nd:YAG laser (532 nm, 10 Hz, 8 ns, 60 mJ per pulse) for 20 min. The focused spot was scanned continually across the pellet surface. The generated soot was flushed back downstream by flowing argon/helium gas and was collected on a quartz substrate, which was placed on a finger outside the oven. The gas flow rate was set to 200 $cm^3\ min^{-1}$ at atmospheric pressure. Numerous attempts to purify the nanooctahedra from the rest of the nanoparticles were carried out, however unsuccessfully so far. More details of the synthesis of MoS_2 nanostructures are presented elsewhere.[2,15]

(10) Golberg, D.; Bando, Y.; Stephan, O.; Kurashima, K. *Appl. Phys. Lett*. **1998**, *73*, 2441–2443.
(11) Stephan, O.; Bando, Y.; Loiseau, A.; Willaime, F.; Shramchenko, N.; Tamiya, T.; Sato, T. *Appl. Phys. A: Mater. Sci. Process*. **1998**, *67*, 107–111.
(12) Seifert, G.; Fowler, P. W.; Mitchell, D.; Porezag, D.; Frauenheim, T. *Chem. Phys. Lett*. **1997**, *268*, 352–358.
(13) Parilla, P. A.; Dillon, A. C.; Jones, K. M.; Riker, G.; Schulz, D. L.; Ginley, D. S.; Heben, M. J. *Nature* **1999**, *397*, 114.
(14) Parilla, P. A.; Dillon, A. C.; Parkinson, B. A.; Jones, K. M.; Alleman, J.; Riker, G.; Ginley, D. S.; Heben, M. J. *J. Phys. Chem. B* **2004**, *108*, 6197–6207.
(15) Bar-Sadan, M.; Enyashin, A. N.; Gemming, S.; Popovitz-Biro, R.; Hong, S. Y.; Prior, Y.; Tenne, R.; Seifert, G. *J. Phys. Chem. B* **2006**, *110*, 25399–25410.
(16) Bar Sadan, M.; Houben, L.; Wolf, S. G.; Enyashin, A.; Seifert, G.; Tenne, R.; Urban, K. *Nano Lett*. **2008**, *8*, 891–896.
(17) Gordon, J. M.; Katz, E. A.; Feuermann, D.; Albu-Yaron, A.; Levy, M.; Tenne, R. *J. Mater. Chem*. **2008**, *18*, 458–462.
(18) Sano, N.; Wang, H.; Chhowalla, M.; Alexandrou, I.; Amaratunga, G. A. J.; Naito, M.; Kanki, T. *Chem. Phys. Lett*. **2003**, *368*, 331–337.
(19) Enyashin, A. N.; Seifert, G. *Phys. Status Solidi B* **2005**, *242*, 1361–1370.
(20) Sen, R.; Govindaraj, A.; Suenaga, K.; Suzuki, S.; Kataura, H.; Iijima, S.; Achiba, Y. *Chem. Phys. Lett*. **2001**, *340*, 242–248.

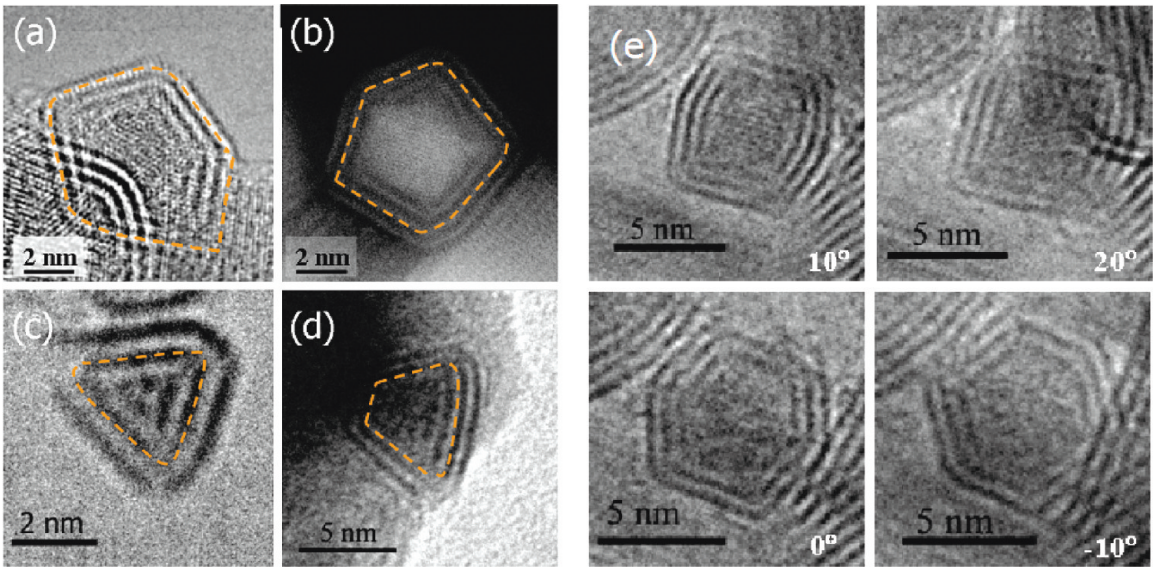

Figure 1. HRTEM (a) and HAADF STEM (b) images showing a pentagonal projection of a MoS_2 nanostructure produced by laser ablation. A TEM image showing a triangular projection of a $MoSe_2$ particle is presented in (c) and a trapezoidal projection of a MoS_2 particle in (d). TEM images of symmetric nanooctahedra, tilted in various angles (ref 15), showing only rhombic and hexagonal projections (e). The dashed orange lines serve as means to guide the eye to the projection morphology.

Microscopy. Extensive work with HRTEM in the past shows that fullerene-like MoS_2 nanoparticles and nanotubes are very stable with respect to beam damage under normal working conditions. For samples selected for TEM, the collected powder was sonicated in ethanol, placed on a carbon/collodion-coated Cu grid, and analyzed by TEM (Philips CM-120, 120 kV).

HRTEM data of MoS_2 nanoparticles were acquired in an FEI Titan 80−300 transmission electron microscope equipped with a double-hexapole aberration-corrector[21] for the objective lens. For single images, negative spherical-aberration imaging (NCSI) conditions[22,23] were adjusted. At 80 kV acceleration voltage, the NCSI conditions are achieved at a negative spherical aberration of $-52\,\mu$m balanced by an overfocus of +17 nm. At 300 kV acceleration voltage the respective values for the NCSI conditions are $-12\,\mu$m and +5 nm.

Some samples were also examined at 300 kV in a JEOL JEM-3000F field emission gun HRTEM, which has a spherical aberration coefficient (C_s) of 0.57 mm and a point resolution of 0.16 nm. Images were acquired digitally on a Gatan model 794 (1k × 1k) CCD camera, and the magnification was calibrated accurately using Si ⟨110⟩ lattice fringes. Focal series were obtained from suitable thin regions, and off-line, the complex exit plane wave function was reconstructed from a 20-image through focal series according to an established procedure.[24−27]

High-angle annular dark field (HAADF) STEM images were taken in an FEI Titan 80−300 electron microscope equipped with a probe-side double-hexapole aberration corrector at an acceleration voltage of 300 kV. The probe forming lens aberration was corrected to a beam semiangle of 25 mrad yielding a probe size better than 0.8 Å. An inner collection angle of 70 mrad of the HAADF detector assured the collection of high-angle deflected electrons that were scattered close to the atomic nuclei.

Simulated TEM images were calculated from supercell data containing the atomic coordinates of computed model structures. The supercells were divided into stacks of 0.2-nm-thick slices for the multislice calculation of the electron wave propagation within the sample. The multislice iteration and electron optical imaging were calculated using the EMS image calculation software.[28]

Computational Methods. All stability and electronic structure calculations were performed using the density-functional-based tight-binding method (DFTB)[29−31] with an a posteriori empirical dispersion correction term, parametrized in the framework of the universal force-field (UFF) method.[32] Prior to full geometry optimization with the DFTB method, the structures were preoptimized with a proprietary molecular mechanics (MM) force field. Finally, the stability of the optimized structures was verified by molecular dynamics (MD) simulations within the DFTB approach.

3. Results

3.1. Recognition of 3D Models of Distorted Octahedra. Previous work focused on the structure of symmetric nanooctahedra and their physical properties.[2,15,16,34] An octahedron is a rectangular bipyramid, and its different projections, as seen in the TEM images, are diamond or hexagon shapes while pentagonal or triangular projections are impossible in any viewing direction. However, experimental HRTEM images showed triangular and pentagonal projections of MoS_2 structures found in the soot of the laser-ablated material (Figure 1). In Figure 1a,

(21) Haider, M.; Uhlemann, S.; Schwan, E.; Rose, H.; Kabius, B.; Urban, K. *Nature* **1998**, *392*, 768–769.
(22) Jia, C. L.; Lentzen, M.; Urban, K. *Science* **2003**, *299*, 870–873.
(23) Lentzen, M. *Microsc. Microanal.* **2006**, *12*, 191–205.
(24) Coene, W.; Janssen, G.; Debeeck, M. O.; Vandyck, D. *Phys. Rev. Lett.* **1992**, *69*, 3743–3746.
(25) Kirkland, A. I.; Meyer, R. R. *Microsc. Microanal.* **2004**, *10*, 401–413.
(26) Meyer, R. R.; Kirkland, A. I.; Saxton, W. O. *Ultramicroscopy* **2004**, *99*, 115–123.
(27) Meyer, R. R.; Kirkland, A. I.; Saxton, W. O. *Ultramicroscopy* **2002**, *92*, 89–109.
(28) Stadelmann, P. A. *Ultramicroscopy* **1987**, *21*, 131–145.
(29) Seifert, G. *J. Phys. Chem. A* **2007**, *111*, 5609–5613.
(30) Seifert, G.; Porezag, D.; Frauenheim, T. *Int. J. Quantum Chem.* **1996**, *58*, 185–192.
(31) Porezag, D.; Frauenheim, T.; Koehler, T.; Seifert, G.; Kaschner, R. *Phys. Rev. B* **1995**, *51*, 12947.
(32) Zhechkov, L.; Heine, T.; Patchkovskii, S.; Seifert, G.; Duarte, H. A. *J. Chem. Theory Comput.* **2005**, *1*, 841–847.

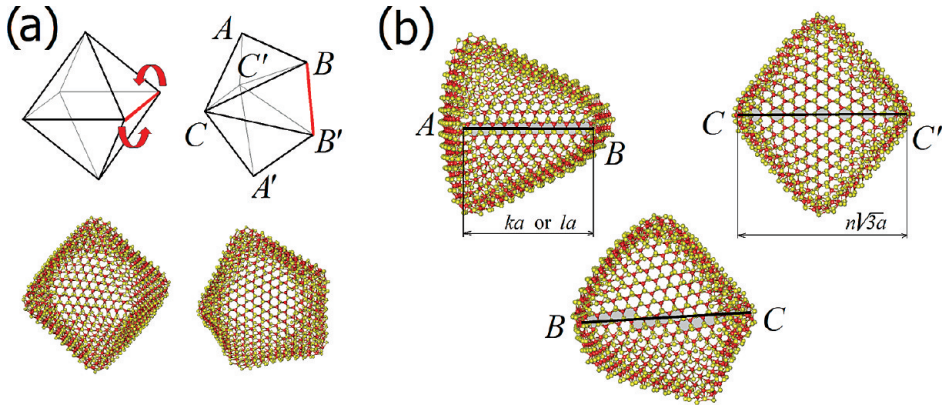

Figure 2. Schematic representation of the morphology of distorted nanooctahedra and the relationship to a perfect octahedron (a). The model can be viewed from several directions, as shown in (b) according to the front edge in each direction. The relation between the indexes n, k, l of the fullerene edge length and the lattice parameter a of bulk MoS_2 is shown.

a HRTEM image of a pentagonal projection of a MoS_2 nanostructure produced by laser ablation is shown. Figure 1b presents an image acquired by HAADF STEM, where the sensitivity for the light atoms (*S*) is lost and the intensity is produced mainly by the heavier element (Mo) alone. In this imaging mode, the structural skeleton is exposed. A conventional TEM image showing a triangular projection of a $MoSe_2$ particle is presented in Figure 1c, and a trapezoidal projection of a MoS_2 particle is presented in Figure 1d. The assumption that symmetric structures are more stable due to the more equally distributed strain within their cages would suggest that trigonal projections should be associated with tetrahedrons or trigonal bipyramids. Pentagonal projections could relate, respectively, to pentagonal bipyramids. However, the construction of these particles would require a defect with an odd number of atoms, three-member rings or five-member rings, at the apex of the structure. Creating such defects in the lattice structure would essentially require a change of the stoichiometry which is highly unlikely.

The presence of nanoparticles with atypical (i.e., non-hexagonal and nonrhombic) cross sections alongside octahedral-shaped structures indicates that both are related by common structural features in their respective microstructure. The octahedral shape of inorganic fullerenes can be explained by the presence of six corners consisting of a square-like defect that results in an overall closed cage structure. To complete the structure, the facets of the octahedron are therefore composed of triangular fragments of a hexagonal monolayer. Thus, six square-like defects are enough to make a closed particle.

The same condition—the presence of six square-like defects—should also be accomplished for particles with an irregular, asymmetric shape. Nevertheless, they will contain fragments with higher or smaller strain energies, which are not optimally distributed over the particle surface. Such particles will have an overall higher total energy. Therefore, under equilibrium conditions the formation of such irregularly shaped particles will tend to be suppressed. However, under nonequilibrium (i.e., fast-growth) conditions they may be formed, though with a smaller probability than the regularly shaped particles. Indeed, a smaller concentration of irregular particles compared to the nanooctahedra is found experimentally. It can be realized that the high cooling rate imposed by the laser pulse forces the ablated plume to condense very rapidly, not allowing enough annealing time to form symmetric structures.

Among the large number of possible arrangements of six square-like defects within a particle shell, we chose the simplest, since it is the closest to the symmetric nanooctahedron: changing the positions of two defects by rotating one of the octahedron's edges by 90° (Figure 2a, marked in red). The change in the morphology inevitably causes changes in the construction of the edges and the facets, although the number of facets is preserved. In symmetric octahedral nanoparticles there are two edge types: edges formed between facets on the same side of the basal plane and edges formed between facets across the basal plane. In contrast, irregular nanoparticles contain at least three different types of edge constructions between the now rotated facets (Figure 2). The orientation of the lattice relative to the edge may be orthogonal or parallel to an edge (i.e., the facets may have either *armchair*- or *zigzag*-like edges) or may even take an intermediate case (Figure 2b). The edge rotation by 90° in Figure 2 produces the vertices A and A', in which three facets are connected. The connecting defect is still square-like since the new type of edge construction enables a break in the apparent one-to-one relationship between rhombohedral defects and octahedral morphology. More examples of model structures of distorted nanooctahedra are shown in Figure S1 in the Supporting Information.

The model of a distorted octahedron can adequately explain the large variety of particle projections observed experimentally: triangular, pentagonal, trapezoidal, rhomboidal, and quadratic (Figure 3a). Figure 3b shows a simulated HRTEM image of the pentagonal projection of a distorted nanooctahedron, alongside its calculated projection of the electrostatic potential (Figure 3c). It is seen that the calculated electrostatic potential is closely related to the experimental HAADF STEM contrast of

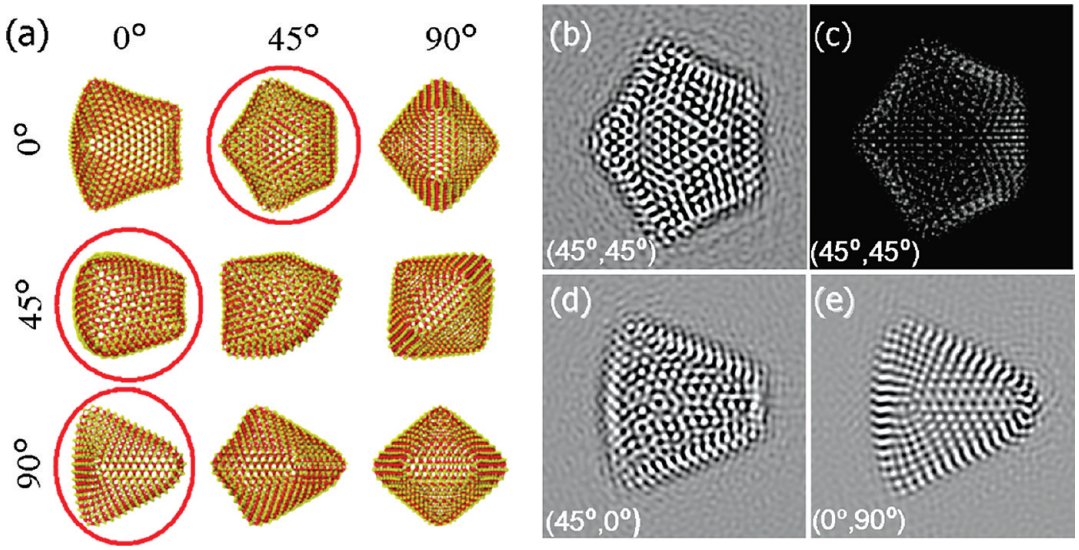

Figure 3. Various orientations of a distorted MoS_2 nanooctahedron model (a). HRTEM image simulation is shown, corresponding to the circled orientations of the structure model (b, d, e). The images were calculated for negative spherical aberration conditions, so that atoms are represented as white relative to the background. A projection of the electrostatic potential of a distorted MoS_2 nanooctahedron, showing the pentagonal orientation, is shown in (c). It is seen that the calculated electrostatic potential is closely related to the experimental HAADF STEM image in Figure 1b, and the simulated HRTEM images correspond to the experimental TEM images presented in Figure 1.

a single shell nanostructure in Figure 1b. Simulated HRTEM images of other orientations of the same proposed structure, circled in red in Figure 3a, are also presented in Figure 3d,e. The correspondence between the simulated HRTEM images in Figure 2 and the obtained experimental images in Figure 1 provides good support for the suggested structure.

In the present study, we restrict the discussion to possible structures with symmetric triangular projections to match those which were observed experimentally, although a huge number of possible structures exist when varying the size and edge proportions. This implies $AC = A'C = AC' = A'C'$ (see Figure 2) and varying only the edge lengths AB, $A'B'$, BB', and so forth. In this case, three integer numbers n, k, and l are sufficient to characterize the size of the particle. The physical meaning of the integer numbers is the number of hexagons forming the edges CC' (which is actually a curved facet), AB ,and $A'B'$. The total number of atoms (N) forming a shell is then determined by the following relation:

$$N = 3(13n^2 - 8n - (l+1)^2 - (k+1)^2 + 1) \qquad (1)$$

3.2. Creation of 3D Models of Nanoseashell Structures. Both the symmetric nanooctahedra and the distorted ones have flat facets, which are closer to the 2D layers observed in the bulk phase. This adds to their relative stability, but the sharp edges and especially the corners which are produced by the lattice defect introduce significant strain into the structure, relative to that observed in either spherical particles or nanotubes. A possible consequence of this higher strain energy can be a reduced tendency to form square-like defects. In such a case, a particle that starts to form around such a defect, which will become the apex of the structure, can grow two asymmetric edges if the introduction of new defects takes place at different speeds. When new defects are introduced and more facets are grown, it may happen that the facets are unable to close upon themselves, and they produce a scroll-like structure which resembles a spiral seashell. Such nanoseashells possess several types of atoms within a single cage: atoms of facets, of edges, and of corners and atoms with dangling bonds, which form the inner edge in the core and the outer edge. In this case, the external edge is capable of continuous growth. Scroll-like morphology is reported in the literature for one-dimensional structures like VO_x nanotubes,[33] for example. In the present study, the scroll is found for a zero-dimensional case. A simple model of a nanoseashell can be built by merging two adjacent shells of a perfect nanooctahedron; cutting two edges of every octahedron within a multiwalled fullerene followed by shifting and attachment of an inner octahedron to the next outer one using the dangling bonds. In such a way, the projections of nanoseashells with a few curls demonstrate amazing similarity to their symmetric nanooctahedra analogues (Figure 4). It can be speculated that the resemblance between the symmetric nanooctahedra and the nanoseashells obstructs their differentiation in conventional TEM microscopes and the variety of the particles can be more diverse than previously assumed.

In Figure 5 we see an experimental example of a nanoseashell. In Figure 5a and (b) HRTEM imaging confirms the scroll-like morphology of the folded structure, and we assume that this structure results from the central plane of the nanoshell alluded to above. In the reconstructed phase image (Figure 5b and see also detail Figure 5d), which is

(33) Krumeich, F.; Muhr, H. J.; Niederberger, M.; Bieri, F.; Schnyder, B.; Nesper, R. *J. Am. Chem. Soc.* **1999**, *121*(36), 8324–8331.
(34) Bar Sadan, M.; Houben, L.; Enyashin, A. N.; Seifert, G.; Tenne, R. *Proc. Natl. Acad. Sci. U.S.A.* **2008**, *105*(41), 15643–15648.

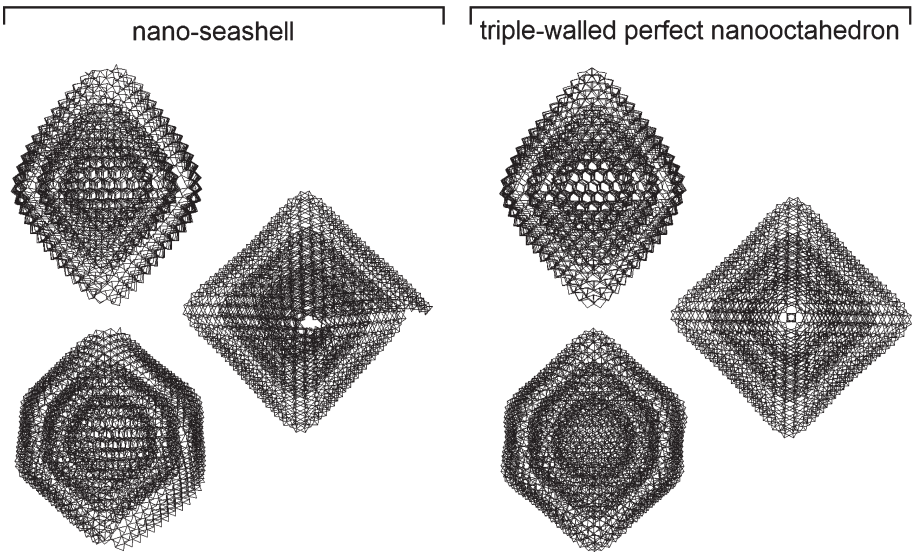

Figure 4. Comparison between the models of a nanoseashell $(MoS_2)_{1328}$ (on the left) and a symmetric nanooctahedron $(MoS_2)_{144}@(MoS_2)_{400}@(MoS_2)_{784}$ (on the right), viewed in different orientations.

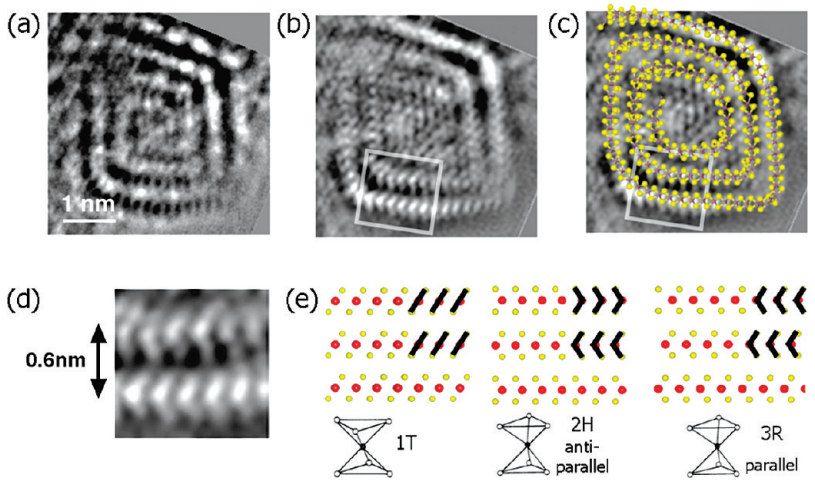

Figure 5. (a) Conventional Scherzer defocus HRTEM image of a nanoseashell. (b) Reconstructed phase image produced from a focal series of images obtained from the same specimen. (c) Central plane of a matching model structure of a nanoseashell. (d) Detail from the reconstructed phase in (b) showing a chevron pattern due to the inner Mo monolayer pair and outer S layer pairs. (e) Models showing the three bulk crystal structure of MoS_2: 1T, 2H, and 3R (Mo and S atoms are in red and in yellow, respectively).

more sensitive to the lighter S atoms in the structure, we see S−Mo−S chevron patterns in adjacent layers apparently in parallel alignment. To understand the atomic configuration inside the shells and between the shells, three bulk crystal structures are presented as Figure 5d: 1T, 2H, and 3R: The 1T-structure consists of an octahedral coordination between a Mo atom and six sulfur atoms surrounding it. Such a configuration produces a diagonal S−Mo−S pattern in projection, marked in black over the structure model, and, as such, does not fit to the experimentally obtained contrast. A corresponding projection pattern based on the 2H layer stacking shows an antiparallel alignment of S−Mo−S chevrons and does not fit either. The parallel alignment of S−Mo−S chevrons produced by the projection of the 3R layer stacking provides a much better fit. The conclusion is that the nanoseashell is constructed from the trigonal prismatic configuration with a parallel alignment of the S−Mo−S chevrons.

From the evidence of the S−Mo−S stacking within the nanoparticle in Figure 5, we can now consider the stacking between MoS_2 layers in nanoparticles in general. Although the 2H-phase and the 3R-phase are illustrated for clarification, it is hardly possible to use these stacking terms when closed low dimensional nanoparticles are concerned, since the individual MoS_2 layers are no longer free to move relative to each other as is possible in the bulk or even for nanotubes, in which the constituent cylinders can move with respect to one another along the tube axis. Furthermore, the translation vector between equivalent atoms in different layers is not constant along the shell structure, since the different shells need to adjust themselves to fit within each other. Hence the discussion can be limited to the presence of a parallel or antiparallel S−Mo−S chevron pattern. It is obvious,that an antiparallel alignment is impossible within a scroll structure; therefore, the parallel chevron pattern supports

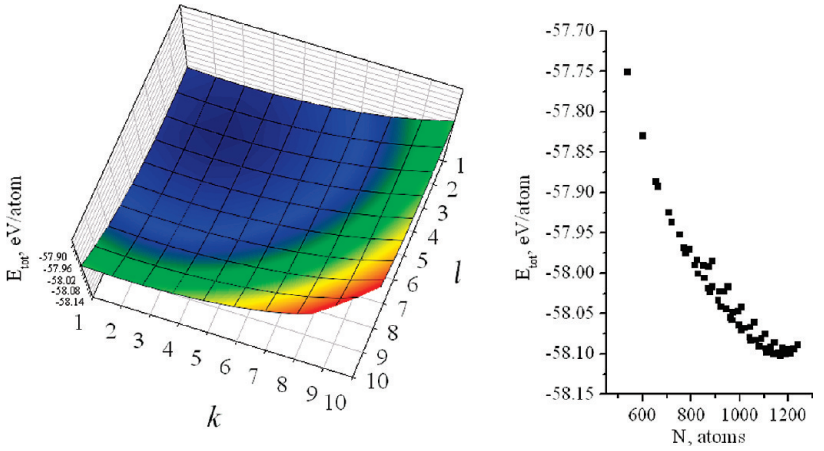

Figure 6. Energy per atom (E_{tot}) of distorted MoS_2 nanooctahedra is shown on the left as a function of their edge lengths n, k, and l representing the number of Mo−S hexagons in each edge [CC', AB, and $A'B'$, see Figure 2]. In this graph, the case $n = 6$ is depicted. The fields with lowest energy are colored in violet. The dependence of the energy per atom (E_{tot}) of distorted MoS_2 nanooctahedra on the total number of atoms N is presented on the right.

the suggested model. It is worth noting that this form of parallel MoS_2 layer stacking is not thermodynamically stable and is rarely encountered in the bulk as in the 3R-MoS_2 phase. The 3R-stacking was reported also for MoS_2 nanotubes and IF-MoS_2 which crystallized within MoS_2 nanotubes.[35,36]However, this kind of stacking cannot be attributed to the stacking in a nanoseashell due to an incommensurability between interlayer distances and difference in the perimeters of neighboring curls (see structural model on Figure 5c). Such a genuine architecture of a seashell possessing uncorrelated layers allows us to characterize the resulting MoS_2 phase as turbostratic-like.

3.3. Stability of Nonoctahedral MoS_2 Fullerenes. We studied 126 different particle structures with the following edge lengths: n between 3 and 6 and k and l up to 10. The total number of atoms was varied from 132 up to 1239. After geometry optimization the separation of 1−2 sulfur atoms from the structure tips was observed. Additional MD simulations at 300 K within the DFTB approach have shown the formation of holes and splits at the corners of the structures (Supporting Information Figure S2). It should be pointed out that the largest splits are obtained at the sharpest tips of the structures, that is, in the areas with the highest strain energies in a similar way to that found for the octahedral nanostructures.[15]

The energies E_{tot} of the distorted MoS_2 nanooctahedra can be plotted as a function of the edge length indexes n, k, and l (Figure 6, Supporting Information Figure S3). The most stable particles among all the structures studied were those having $k = 3$ and $l = 3$. We did not find any clearly expressed dependence of the energy E_{tot} on all parameters n, k, l together. It can be seen that for small nanoparticles with $n = 3$ to 5, a uniform distribution in the energies depending on k and l was not observed, so that a local minimum on the E_{tot} surface can be found. The most indicative example is a small $(MoS_2)_{112}$ fullerene with $n = 4$, $k = 3$, and $l = 6$ that has an energy comparable to its related elongated $(MoS_2)_{145}$ fullerene, which consists of a larger number of atoms and with the indices $n = 4$, $k = 3$, and $l = 3$.

Practical interest is attached to the largest fullerenes considered here ($n = 6$). The most stable system is $(MoS_2)_{389}$ with $k = 3$ and $l = 3$. It is noticeable that the most stable particle is neither that with the sharpest A and A′ and most obtuse B and B′ corners nor with the sharpest B and B′ and most obtuse A and A′ corners, but some intermediate case, which has a lower strain energy. However, the largest stable particle considered in the theoretical investigations does not have a perfect pentagonal-like cross section like the one found in the experiment. This can be explained by the fact that the calculations cannot include larger nanoparticles, which are composed of many thousands of atoms and are multilayered like the ones observed experimentally. Nevertheless, the calculations show that for particles with $n = 6$ there is already a smoothed dependence of E_{tot} on k and l, which has only one minimum (Figure 6). The absence of any other local minimum enables a phenomenological model based on the elasticity theory to be applied in the future. This model could be valid for particles with approximately 1000 atoms and more.

The present calculations of the geometries and energies supply a set of 126 particles of the same MoS_2 composition, at a temperature $T = 0$ K. An estimation of the relative concentrations of the particles at nonzero temperatures can be compared with the experimental data, in a similar approach to the one already used for the case of isomeric carbon fullerenes.[37,38] The relative concentrations can be expressed using simple Boltzmann factors as the mole fractions w_i of MoS_2 within a specific particle. Then, energy values (ΔE_i) of m particles, which can be calculated relative to the most stable particle, can be analyzed by Boltzmann statistics to estimate the fraction

(35) Remškar, M.; Škraba, Z.; Ballif, C.; Sanjines, R.; Levy, F. *Surf. Sci.* **1999**, *433−435*, 637–641.
(36) Remškar, M.; Mrzel, A.; Virsek, M.; Jesih, A. *Adv. Mater.* **2007**, *19*, 4276–4278.
(37) Slanina, Z.; Lee, S. L.; Adamowicz, L. *Int. J. Quantum Chem.* **1997**, *63*, 529–535.
(38) Slanina, Z.; Lee, S. L.; Yoshida, M.; Osawa, E. *Chem. Phys.* **1996**, *209*, 13–18.

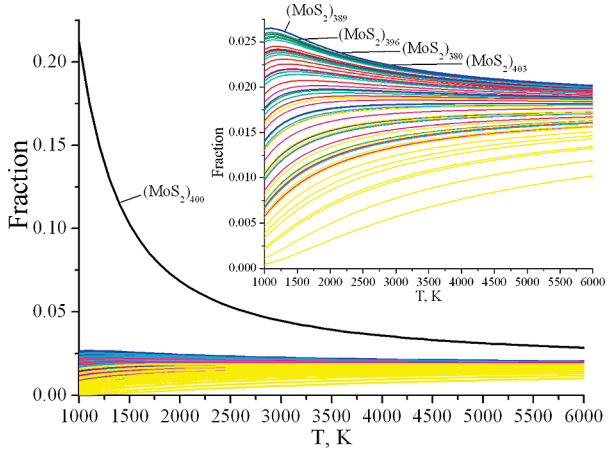

Figure 7. Quasi-equilibrium distribution functions of nanooctahedra calculated for an assessment of the distribution of morphologies in a soot produced by laser ablation. The distribution functions show the fraction of different structure species as a function of temperature. In particular, this graph compares the fraction of a symmetric octahedral fullerene $(MoS_2)_{400}$ versus 55 distorted MoS_2 nanooctahedra of approximately the same size (with a close number of atoms). In the inset, an enlarged portion of the graph is presented, where the fractions are less than 2.5%.

of the distorted nanooctahedra relative to the symmetric octahedral fullerenes:

$$w_i = \frac{\exp(-\Delta E_i/kT)}{\sum_{i=1}^{m} \exp(-\Delta E_i/kT)} \qquad (2)$$

Since the number of possible combinations comparing the ideal nanooctahedron with its corresponding distorted structures is high, the discussion will be limited to one case study. In this case, the $(MoS_2)_{400}$ nanooctahedron will be compared with distorted MoS_2 octahedra of a similar size, with $n = 6$ and $N = 537$ to 1239 atoms. Despite its great simplicity, such a quasi-equilibrium model gives semiquantitative information at each temperature about the distribution functions for nanooctahedra. The distribution of morphologies in the soot produced by the laser ablation will reflect these quasi-equilibrium distributions according to the process temperatures involved in the laser ablation. The model agrees well with the relative distributions of rhombic and hexagonal cross sections, which can be attributed to any morphology of nanooctahedra, versus pentagonal and triangular cross sections belonging exclusively to distorted nanooctahedra. Moreover, it shows a trend in the change of fraction for different structure species as a function of temperature (Figure 7).

It appears that the symmetric fullerene $(MoS_2)_{400}$ is by far the most stable and most abundant in the temperature range checked. Its fraction at 1000 K is about 21%, while other distorted structures are produced in much lower quantities of 0 to 2.5% each. The most stable among them are the fullerenes: $(MoS_2)_{389}$ (with $k = 3$, $l = 3$), $(MoS_2)_{396}$ (with $k = 2$, $l = 3$), $(MoS_2)_{380}$ (with $k = 3$, $l = 4$), and $(MoS_2)_{403}$ (with $k = 2$, $l = 2$). However, the fraction of the $(MoS_2)_{400}$ fullerenes rapidly decreases as the temperature increases. At 2500 K, the fraction of the $(MoS_2)_{400}$ fullerenes is only 5%, whereas the fraction of the distorted structures is not that drastically changed. At higher temperatures, the fraction of $(MoS_2)_{400}$ is comparable with the distorted species and does not exceed 3%.

In the case of the nanoseashells, the problem of time- and resource-consuming calculations hinders the direct comparison of the stability of nanoseashells with that of multiwalled octahedral fullerenes by quantum mechanical methods. In the nanoseashell case, the number of atoms in a single curl of the structure grows rapidly: the number of atoms in an inner curl k would become proportional to $\sim k^2$ in its next external curl. Nevertheless, the stability of such structures can be discussed on the basis of a phenomenological model, where an equation describing the dependence of the energy as a function of size and structural characteristics of a nanoseashell is considered in this way, as was done previously for the nanooctahedra and other IF structures.[2,15] The energy per atom, E_{tot}, for a nanoseashell can be expressed as the sum

$$NE_{tot} = N_\infty \varepsilon_\infty + N_r \varepsilon_r + N_x \varepsilon_x + N_p \varepsilon_p \qquad (3)$$

where N is the total number of atoms, Mo and S. N_∞, N_r, N_x, and N_p are the numbers of Mo and S atoms at the faces, at edges without dangling bonds, at edges with dangling bonds, and at the corners (represented by square-like defects), respectively. The corresponding energies per atom are ε_∞, ε_r, ε_x, and ε_p. The total number of atoms, N, which make up a nanoseashell of k curls and the following numbers: N_∞, N_r, N_x, and N_p, can be found in the following way. Using the number of atoms within the ith curl N_i:

$$N = \sum_{i=1}^{k} N_i$$

$$N_\infty = \sum_{i=1}^{k} (N_i - 6\sqrt{N_i}) - \sqrt{N_i} + 6k + 3$$

$$N_r = 6\sum_{i=1}^{k} \sqrt{N_i} - \sqrt{N_k} - 30k$$

$$N_r = 6\sum_{i=1}^{k} \sqrt{N_i} - \sqrt{N_k} - 30k$$

$$N_r = \sqrt{N_1} + \sqrt{N_k} + 3$$

$$N_p = 24k - 6 \qquad (4)$$

The difference between the numbers of atoms in two adjacent curls, N_i and N_{i-1}, may be determined using the

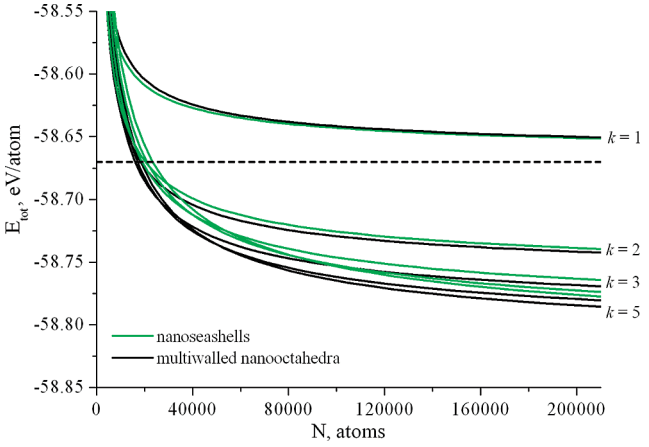

Figure 8. Dependence of the energy E_{tot} on the total number of atoms N for MoS_2 nanoseashells (in green) and MoS_2 octahedral fullerenes (in black), where the number k represents the number of curls or walls, respectively.

equation for a multilayered nanooctahedron,[15] where a and c are the lattice constants of bulk 2H-MoS_2:

$$\sqrt{N_i} - \sqrt{N_{i-1}} = 3\sqrt{2}\frac{c}{a} \qquad (5)$$

The van der Waals interactions can be incorporated into eq 3 by adding the term $(N-N_k)\varepsilon_{vdW}$ as the energy of interaction between the walls of two curls. A comparison of the energy E_{tot}, as calculated by the phenomenological model for the symmetric nanooctahedra and the nanoseashells, is presented in Figure 8. The graph presents the energy values for nanooctahedra with one to five shells, and the corresponding nanoseashells with one to five curls ($k = 1-5$). It can be seen that when the structures have one or two shells/curls, the difference between the energies of these two kinds of nanoparticles is insignificant. In fact, at $k = 1$, the nanoseashell can be imaged as a cracked fullerene. Evidently, the disappearance of three square-like defects in the structure is compensated by the appearance of four edges with dangling bonds. However, at larger numbers of shells/curls (high values of k), the difference between the total energies of the nanooctahedra and the nanoseashells becomes larger, and the nanoseashells are less stable. Thus, the probability of finding a nanoseashell with numerous curls will be lower than that of finding nanooctahedra with the same number of walls.

3.4. Electronic Structure. To understand the influence of the morphology of the nanoparticles on its electronic structure, calculations of the densities of states (DOS) were performed on particular cases for a distorted nanooctahedron $(MoS_2)_{389}$, a symmetric nanooctahedron $(MoS_2)_{400}$, and a nanoseashell $(MoS_2)_{408}$, which have roughly the same size (Figure 9). The DOS profiles of all three nanoparticles are similar to those of semiconducting MoS_2 nanotubes and the corresponding bulk layered 2H-structure with one distinct difference: these structures are characterized by a metal-like character of the DOS, independent of the morphology of the particles. The HOMO−LUMO gap does not exceed 0.01 eV,

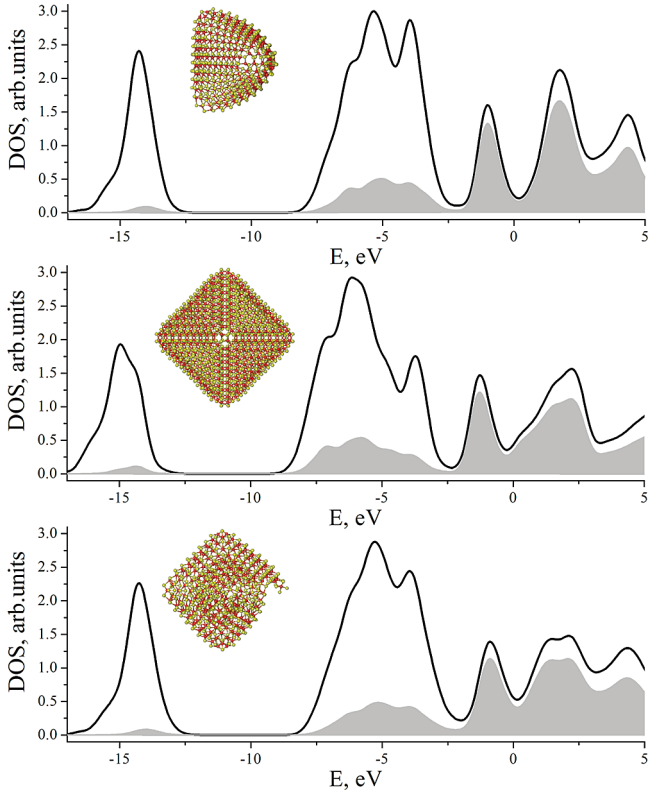

Figure 9. Electronic density of state (DOS) calculated for a distorted nanooctahedron $(MoS_2)_{389}$, a symmetric nanoctahedron $(MoS_2)_{400}$, and a nanoseashell $(MoS_2)_{408}$ (from top to bottom). The total density of states is drawn as a solid line and Mo 4d partial densities of state are plotted as filled curve. 0.0 eV − HOMO.

and the states around the HOMO−LUMO gap are dominated by Mo 4d states. Thus, distorted nanooctahedra and nanoseashells demonstrate similar features of electronic structure to the symmetric nanooctahedra. The metallic-like nature of the DOS may be an indirect indication of the high catalytic reactivity of MoS_2 fullerenes, which could be comparable with that of single layer triangular MoS_2 nanoplatelets. These unique nanoparticles were characterized as having a metallic-like character due to the dangling bonds at their edges, and they exhibit high catalytic reactivity with respect to the hydrodesulfurization of gasoline and water splitting[39,40] However, to support this speculation further experimental research should be performed.

4. Discussion and Conclusions

Experimental and theoretical findings obtained so far lead to the conclusion that the synthesis carried out close to equilibrium conditions results in an initial quasi-spherical morphology, which changes into a faceted morphology as the thickness of the layered material exceeds a certain ratio.[41,42]

(39) Helveg, S.; Lauritsen, J. V.; Lægsgaard, E.; Stensgaard, I.; Nørskov, J. K.; Clausen, B. S.; Topsøe, H.; Besenbacher, F. *Phys. Rev. Lett.* **2000**, *84*, 951.
(40) Lauritsen, J. V.; Kibsgaard, J.; Helveg, S.; Topsøe, H.; Clausen, B. S.; Lægsgaard, E.; Besenbacher, F. *Nature Nano* **2007**, *2*, 53–58.
(41) Srolovitz, D. J.; Safran, S. A.; Homyonfer, M.; Tenne, R. *Phys. Rev. Lett.* **1995**, *74*, 1779–1782.
(42) Zak, A.; Feldman, Y.; Alperovich, V.; Rosentsveig, R.; Tenne, R. *J. Am. Chem. Soc.* **2000**, *122*, 11108–11116.

The introduction of facets is inherently produced in thicker particles, where they relieve the high strain energies associated with the bent layers of the lattice. Under these conditions, no nanooctahedra have been found to date. It was already concluded in the literature, therefore, that the temperature range 1000 to 1200 K produces a growth phase in the MoS_2/WS_2 systems,[42−44] where the defects mainly originate from strain relief mechanisms.

The new insights in the present work refer to the formation of the nanooctahedra and their related morphology in the higher, nonequilibrium conditions where the system is controlled by the kinetics. In the laser ablation process, some of the target material is simply polished off, creating small platelets of a few tenths of a nanometer. In addition, smaller nanoplatelets and closed-cage faceted cages are formed, probably from the plasma plume. As the "soup" of different species cools down at a very high rate (10^{-9} s), it is carried by Ar gas through an oven at a temperature of about 1000 K. The last annealing stage adds time (about 1 s) for growth and rearrangement of the nanoparticles.

The structural identity of the MoS_2 seed that later forms the octahedral morphology is still unknown. It is possible that the seed is a square-like defect, from which edges and facets start to grow at equal speed (and produce symmetric octahedral structures) or at different speeds, creating a nanoseashell or an asymmetric structure when the edges are capable of closing into shells. In the latter case, strain considerations show that structures with closer angles to the symmetric are more stable. It is also possible that a thin (1−2 monolayers) platelet is introduced with a defect, which causes the structure to relieve strain by creating grain boundaries in the form of edges.

Using HRTEM, the nanoseashell MoS_2 nanostructure was identified for the first time. To our knowledge, these nanoparticles are the first example of zero-dimensional nanostructures with scroll-like morphology. Evidently, their synthesis became possible only due to step-by-step growth from a plasma vapor, in contrast to formerly known one-dimensional nanoscrolls of VO_x or $H_2Ti_3O_7$, which have been fabricated by the rolling of respective planar sheets from the bulk in a solvent.[33,45]

At 1000 K, where rearrangements and growth are possible, the equilibrium of nanostructures fractions shows a higher concentration of symmetric structures. The defects are created more readily at higher temperatures, but then the different structures are most likely annealed at 1000 K, enriching the soot with the symmetric morphology.

In summary, the atomic level structure of several irregular MoS_2 nanostructures was studied in detail. To describe experimentally observed TEM images, which cannot be attributed to the octahedral shape of the nanoparticles, two main deviations from the symmetric model were proposed: distorted nanooctahedra, where the edges of the structure are asymmetric, and a seashell-like scroll structure. The fundamental structural properties of the inorganic lattice were the basis for matching the observed TEM projections with a proposed model. The stability and electronic properties of the suggested structures were investigated by means of a quantum-mechanical method, verifying that even when structures differ from an ideal symmetric structure, their metallic-like character is preserved. Using calculated energies of symmetric and distorted nanooctahedra, a possible reaction route was briefly discussed. It was concluded that the production of symmetric nanooctahedra involves both a high-temperature stage and an annealing stage. Lattice defects, which are needed for the closure of the structures, are most likely produced in the high temperature stage while at lower temperatures, annealing processes enrich the mixture with symmetric structures.

Acknowledgment. The authors wish to thank Prof. R. Tenne from the Weizmann Institute of Science for valuable discussions and ERC Grant INTIF No. 226639 for funding. L.H. and M.B.-S. thank the Deutsche Forschungsgemeinschaft (DFG) for their support of sub-Ångström microscopy at the Ernst Ruska Centre. M.B.-S. would like to acknowledge the Minerva Fellowship program funded by the German Federal Ministry for Education and Research, the support of the GMJ Schmidt Minerva Center for Supramolecular Chemistry, and the support of the Harold Perlman Foundation. J.S. is indebted to the Royal Society for financial support and also to the Department of Materials, Oxford, for access to HRTEM equipment made available by the EPSRC equipment access fund. A.N.E. and G.S. acknowledge the Center for Information Services and High Performance Computing (ZIH TUD) for making computational resources available.

Supporting Information Available: Figure S1 shows a gallery of different morphologies of distorted MoS_2 nanooctahedra, Figure S2 displays graphs of the energies of distorted MoS_2 nanooctahedra as a function of their morphology and size, and Figure S3 shows energies per atom of distorted MoS_2 nanooctahedra (PDF). This material is available free of charge via the Internet at http://pubs.acs.org.

(43) Feldman, Y.; Frey, G. L.; Homyonfer, M.; Lyakhovitskaya, V.; Margulis, L.; Cohen, H.; Hodes, G.; Hutchison, J. L.; Tenne, R. *J. Am. Chem. Soc.* **1996**, *118*, 5362–5367.
(44) Feldman, Y.; Wasserman, E.; Srolovitz, D. J.; Tenne, R. *Science* **1995**, *267*, 222–225.
(45) Chen, Q.; Du, G. H.; Zhang, S.; Peng, L.-M. *Acta Crystallogr., Sect. B* **2002**, *58*, 587–593.